Physica Medica 62 (2019) 53–62

Contents lists available at ScienceDirect

Physica Medica

journal homepage: www.elsevier.com/locate/ejmp

Original paper

TOPAS Monte Carlo simulation for double scattering proton therapy and dosimetric evaluation

Hongdong Liu[a,b], Zuofeng Li[b], Roelf Slopsema[c], Liu Hong[b], Xi Pei[a], Xie George Xu[a,d,*]

[a] Department of Physics, University of Science and Technology of China, Hefei, Anhui, China
[b] University of Florida Health Proton Therapy Institute, Jacksonville, FL, USA
[c] Emory Proton Therapy Center, Atlanta, GA, USA
[d] Nuclear Engineering Program, Rensselaer Polytechnic Institute, Troy, NY, USA

ARTICLE INFO

Keywords:
Monte Carlo
TOPAS
Proton therapy
Double scattering
Range compensator

ABSTRACT

Purpose: To construct and commission a double scattering (DS) proton beam model in TOPAS Monte Carlo (MC) code. Dose comparisons of MC calculations to the measured and treatment planning system (TPS) calculated dose were performed.

Methods: The TOPAS nozzle model was based on the manufacturer blueprints. Nozzle set-up and beam current modulations were calculated using room-specific calibration data. This model was implemented to reproduce pristine peaks, spread-out Bragg peaks (SOBP) and lateral profiles. A stair-shaped target plan in water phantom was calculated and compared to measured data to verify range compensator (RC) modeling.

Results: TOPAS calculated pristine peaks agreed well with measurements, with accuracies of 0.03 cm for range R_{90} and 0.05 cm for distal dose fall-off (DDF). The calculated SOBP range, modulation width and DDF differences between MC calculations and measurements were within 0.05 cm, 0.5 cm and 0.03 cm respectively. MC calculated lateral penumbra agreed well with measured data, with difference less than 0.05 cm. For RC calculation, TPS underestimated the additional depth dose tail due to the nuclear halo effect. Lateral doses by TPS were 10% lower than measurement outside the target, while maximum difference of MC calculation was within 2%. At deeper depths inside the target volume, TPS overestimated doses by up to 25% while TOPAS predicted the dose to within 5% of measurements.

Conclusion: We have successfully developed and commissioned a MC based DS nozzle model. The performance of dose accuracy by TOPAS was superior to TPS, especially for highly inhomogeneous compensator.

1. Introduction

Proton therapy has become increasingly accepted around the world. According to the latest PTCOG statistics, there are currently 77 proton therapy centers in operation worldwide, with 44 new facilities under construction and 20 facilities in plan stage [1]. By the end of 2017, more than 170,000 patients have been treated with proton therapy [2]. Based on how 3D dose distributions are produced, proton therapy delivery methods can be divided as passive scattering, uniform scanning, and pencil beam scanning techniques [3–5]. System nozzles may be designed to produce the so-called “universal nozzle” that allows selective delivery of each one of these techniques. Passive scattering technique, although being replaced by pencil beam scanning (PBS) technique, has been used in treatment of most of proton therapy patients [3]. This manuscript describes the modeling and commissioning of the double scattering technique of a universal nozzle in the Tool for Particle Therapy Simulation (TOPAS) toolkit [6].

The physical characteristics of a proton beam, also known as Bragg peak, allows delivery of prescribed dose to the tumor while minimizing doses to the surrounding normal tissues [7,8]. Full clinical implementation of this physical advantage of proton beam requires highly precise imaging, treatment field setting, patient positioning, and dose calculation [4]. Therapeutic proton beam dose calculations are performed in the treatment planning system (TPS). Currently available commercial treatment planning systems use analytic dose calculation algorithms, such as pencil beam dose algorithms (PBAs) [9,10], to perform DS dose calculations, although MC dose calculations are now available from TPS vendors for PBS beams [11–13]. It has been well-established that the PBAs have limited accuracy for dose calculation in highly inhomogeneous media [14–17]. MC methods are generally considered to allow improved dose calculation accuracy over analytical dose calculation algorithms, and detailed MC simulations of the DS

* Corresponding author at: Department of Physics, University of Science and Technology of China, Hefei, Anhui, China.
E-mail address: xgxu@ustc.edu.cn (X.G. Xu).

https://doi.org/10.1016/j.ejmp.2019.05.001
Received 31 January 2019; Received in revised form 15 April 2019; Accepted 1 May 2019
Available online 09 May 2019

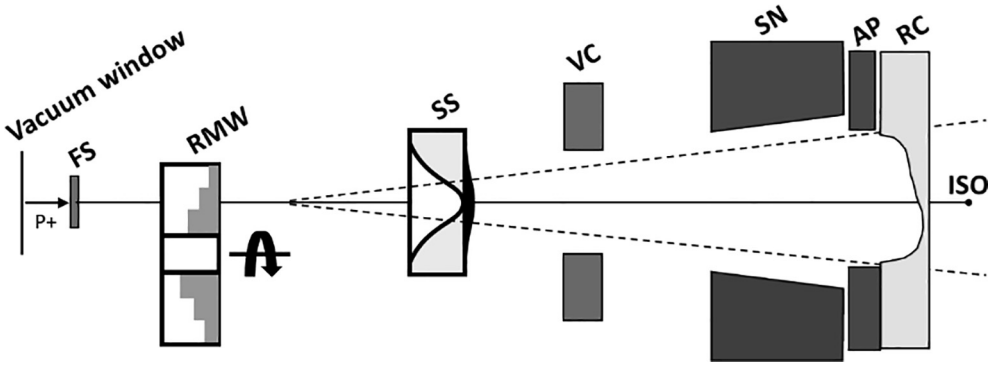

Fig. 1. Simplified schematic illustration of the DS nozzle (not to scale).

Table 1
SOBP ranges and modulation widths available for 8 options.

Option	Min range (cm)	Max range (cm)	Max Modulation width (cm)	Range Modulation ID
B1	4.6	5.87	5.87	#7 (wheel 1, track 3)
B2	5.87	7.49	7.49	#7 (wheel 1, track 3)
B3	7.49	9.55	9.55	#5 (wheel 2, track 2)
B4	9.55	11.65	11.64	#4 (wheel 2, track 1)
B5	11.65	15.54	15.54	#5 (wheel 2, track 2)
B6	15.54	19.83	17.4	#4 (wheel 2, track 1)
B7	19.83	23.91	18	#6 (wheel 2, track 3)
B8	22.8	27.99	15.9	#8 (wheel 3, track 2)

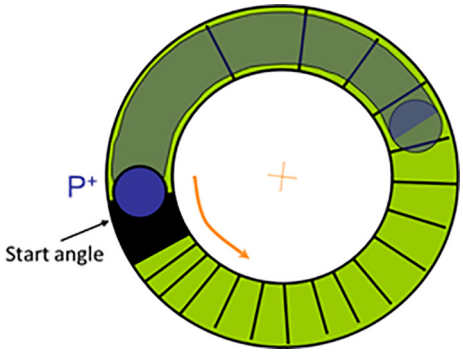

Fig. 2. A brief illustration of the start angle for the RMW track, the black region represents the “stop block”.

treatments have the potential to enhance the accuracy and delivery for proton therapy planning [14,18–22]. Accurate and comprehensive modeling and validation of beam delivery system components is a prerequisite of MC calculations for DS proton therapy. In this study, we developed a DS nozzle model based on manufacturer blueprints by using TOPAS code [6]. TOPAS is a versatile MC platform based on Geant4 [23] and specifically designed for particle beam radiotherapy dose calculations, especially for DS proton therapy [6,24–26]. Multiple studies have implemented the TOPAS code in DS nozzle simulation and demonstrated high dose calculation accuracy [18,21,22]. Such implementations are, however, site-specific and usually rely on use of vendor-proprietary nozzle information. It is therefore necessary for TOPAS users to develop their own machine-specific models and perform validations based on their own beam data measurements.

For DS mode, the high heterogeneities in the beam path mainly come from two aspects: range compensator (RC) and patient anatomy. Some investigators have reported the MC based treatment plan verification for DS patients with various cancer sites, and significant differences between the MC and TPS calculated doses were observed [17,18,20]. The inaccuracy in DS patient treatment plan calculation by TPS was partly from the anatomical heterogeneities and CT calibration, but also in some extent due to the range compensator modelling, which has been lack of concern and rarely investigated thoroughly. MC dose calculations contain the patient specific RC and CT image are usually performed to compare with TPS calculations, but it’s hard to quantitatively distinguish the difference purely from RC, nor hard to validate by measurement. In this work, we presented an experimental validation of a “stair” shaped target in homogeneous water phantom with highly inhomogeneous RC. Comprehensive comparisons of the depth and lateral dose distributions by MC simulation and TPS calculation with measured data were performed.

This study had two goals. The first one was to construct and commission our specific DS nozzle model developed in TOPAS. A series of verifications including pristine Bragg peaks, ranges, distal dose fall-off (DDF) values, spread-out Bragg peaks (SOBP) curves, SOBP range and width, lateral profiles, lateral penumbra values were performed by comparison with measured beam data. The second goal of our study was to evaluate the performance of dose accuracy for TPS and TOPAS with highly inhomogeneous compensator. Both the depth doses and lateral profiles in water have been calculated and compared with the measurements.

2. Materials and methods

2.1. Monte Carlo code and hardware infrastructure

Monte Carlo code TOPAS [6] (version 3.1) was used for the simulation. TOPAS was originally developed by a National Institutes of Health (NIH) funded collaboration of SLAC National Accelerator Laboratory, Massachusetts General Hospital (MGH) and University of California San Francisco (UCSF) [6]. Based on the general MC platform Geant4 [23], TOPAS offers advanced features for complex geometry modeling, material settings, source specifying, physics list and the time-dependent behaviors, all managed through a user-friendly parameter system [6,24–26]. TOPAS allows users to create input parameter files even without a complete knowledge of Geant4 or advanced programming skills, which can greatly reduce time required for beginners learning TOPAS. Most of TOPAS applications have been conducted in proton therapy, especially for DS modality [17,18,20–22]. TOPAS

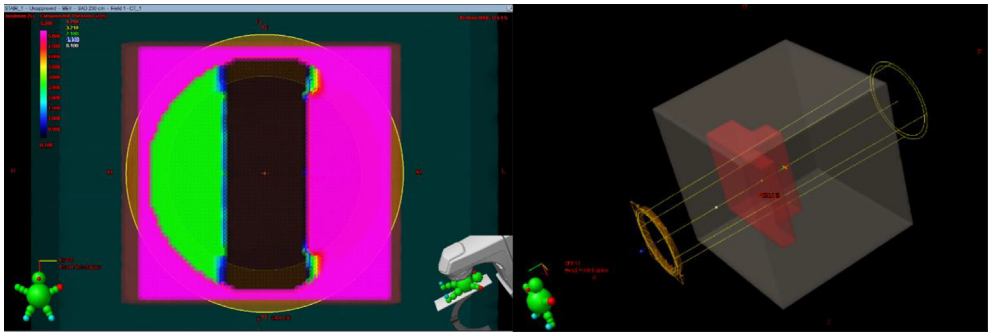

Fig. 3. Cross-section view of the range compensator thickness contour (left) and the "stair-shaped" target (right) in TPS. Different color in left part of this figure represent the various thickness of the RC pixels.

includes a number of predefined components essential for DS nozzle modeling, so that users only need to provide their own set of specific parameters [6]. The TOPAS default physics list was used in this simulation, which has been validated to work well for proton therapy research at MGH [27]. Details about the TOPAS code can be found in the literatures [6,24–26]. All our MC simulations were performed on a Dell workstation with dual Intel Xeon Gold 6138 CPU (40 threads for each) and 128 GB RAM.

2.2. Description of the DS nozzle

Double scattering is a proton therapy delivery technique which uses scatterers and range shifting components to spread proton beams both laterally and depth-wise [3]. Fig. 1 presents a simplified diagram (not to scale) of an IBA (Ion Beam Applications, Belgium) DS nozzle. This model was then constructed in TOPAS based on the parameters provided by manufacturer and previous beam commissioning data. Components like first scatterer (FS), range modulation wheel (RMW), second scatterer (SS), variable collimators (VC), snout (SN), aperture (AP) and range compensator (RC) have been incorporated into the modeling.

The MC simulation starts at the vacuum window before proton beams enter into the nozzle, and distance from vacuum window to the isocenter is approximately 290 cm. The proton beam that exits from vacuum window is nearly mono-energetic, with an initial spot fluence that may be fitted to a Gaussian profile of only a few millimeters in sigma [3]. Clinical use of proton beams requires both spreading the beam in lateral direction as well as creating a uniform dose distribution in depth. In the lateral direction, proton beams are scattered by the fixed scatterers (i.e. the FS) and contoured second scatterer (i.e. the SS) to create a flat profile. FS is a combination of fixed flat scatterers (also called lollipops, made of lead or Lexan), and these lollipops can be independently moved in or out of the beam path, which allows achieving variations of the total thickness of scattering materials for different proton energies. Beam profile after FS is nearly Gaussian-like. In order to obtain a flat profile, the SS is used to scatter more of the central protons to the outside [3]. The SS is consisted of a Lexan base with the lead cap on top, the shape is thick in center and thin on the edge. The combination of high Z (lead) and low Z (Lexan) material in SS is implemented to compensate for the energy loss [3], as protons penetrating through the center of SS will lose more energy than through the periphery. In order to cover all energies, there are three different SS in the DS nozzle.

In the depth direction, a uniform dose region is generated by adding weighted Bragg peaks which are shifted in depths. A rotating RMW synchronized with beam current modulation was employed to achieve this goal [3,28,29]. There are three RMWs in our DS nozzle, located downstream of the FS (see Fig. 1). Each RMW has three sub-tracks, the segmented steps in each track have different thickness, span-angle, and constituent materials [3]. Each step in the track corresponds to a pristine peak in the SOBP. When the RMW rotates in the beam, the steps are sequentially irradiated. Thickness of a step determines the range pullback of the pristine peak, while the angular span of the step determines how many protons will irradiate the step. Beam current modulation, i.e. variation of proton beam current as a function of RMW rotation angle (3.6 deg/ms), is calibrated to correct the angular weights of RMW steps and obtain a uniform SOBP for all ranges [5]. For each SOBP, the specific combination of range and modulation width (defined as the distance between the proximal and distal 90% dose levels), and field diameter, determines which particular track of the RMW, FS, SS, and beam modulations (so called "nozzle setup") will be used. Nozzle setups of all available SOBPs are grouped into options, with a total of 8 in the DS nozzle of this study. The available treatment ranges in our DS nozzle are 4.6 cm–23.9 cm for maximum field size up to 25 cm in diameter. When a uniform field size of 14 cm in diameter or less is requested, the available maximum range can be up to 28.4 cm in water [3,15]. Table 1 shows the ranges and modulation widths combinations as well as the RMW tracks used for each option.

Variable collimators (VC) are used to shape a rectangular field size and also contribute to neutron dose reduction [30]. The VC consists of two pairs of jaws which confine the field size by moving in and out in the X and Y directions. The snout holds additional components, such as the aperture and range compensator. The aperture is used to shape proton doses in lateral direction, while the range compensator conforms proton dose distally. A nozzle-specific conversion algorithm (CONVALGO, IBA) was implemented to determine the nozzle set-up such as FS lollipop combinations, SS selections, RMW track, beam energy, variable collimator opening and beam current modulation file, according to prescribed beam parameters (beam range, SOBP width, field radius, dose rate, etc.).

2.3. Pristine Bragg peaks: Tuning of range and energy spread

Proton energy at the nozzle entrance is one of the key parameters used to derive the beam characteristics. For DS proton dosimetry in clinical applications, the proton range is of greater concerns than the proton energy itself. The CONVALGO algorithm can be used to calculate the required beam energy at nozzle entrance for a prescribed beam range. Direct application of this conversion is however inappropriate for MC simulations, as incorrect beam range may be calculated, due to the following reasons: it is impractical to perfectly reconstruct every single aspect of the beam delivery system, such as the second scatterers modeling, their irregular shapes were approximated with geometries capable to model in TOPAS; it is also difficult to obtain accurate estimates of the initial beam optical properties such as the energy and momentum distributions [29]. To derive the proper energy-range relationship for the MC calculation, comparisons of calculated vs. measured pristine Bragg peaks must be performed under the specific nozzle configuration, with energy corrections made in MC simulations as appropriate. In this step, we set up the FS lollipops and SS using the

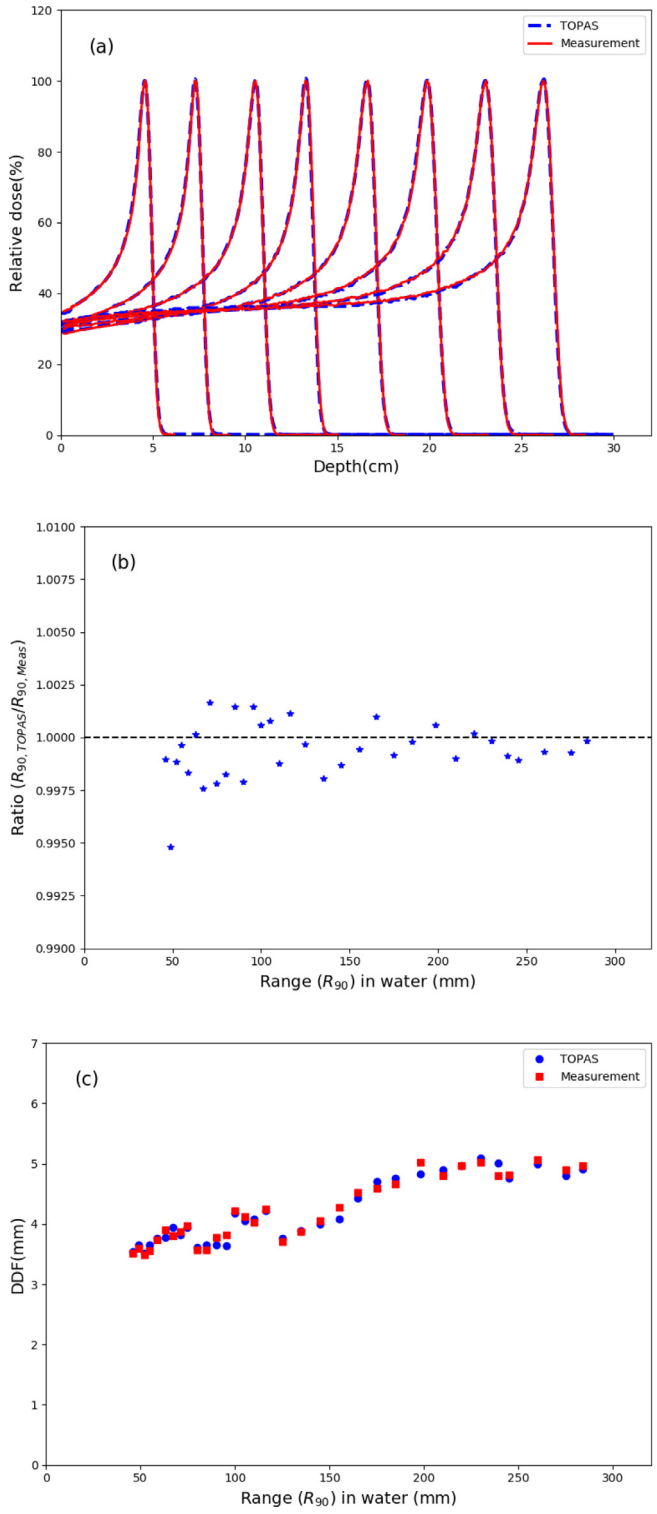

Fig. 4. Verification of pristine Bragg peaks. (a): Normalized TOPAS calculation vs. measurements. (b): Ratios of TOPAS calculated R_{90} over measurement. (c): The distal 80–20% DDF vary with the range.

CONVALGO, but kept the RMW static so that only the first track was irradiated. No aperture and range compensator was used in this step. MC simulation was performed with the same nozzle setup and assumed that the primary incident proton pencil beam had Gaussian distributions of particle fluence, energy spread, and angular spread. The initial Gaussian standard deviation of the spot fluence and angular spread were 0.6 cm and 0.003 rad respectively. This beam phase space data is

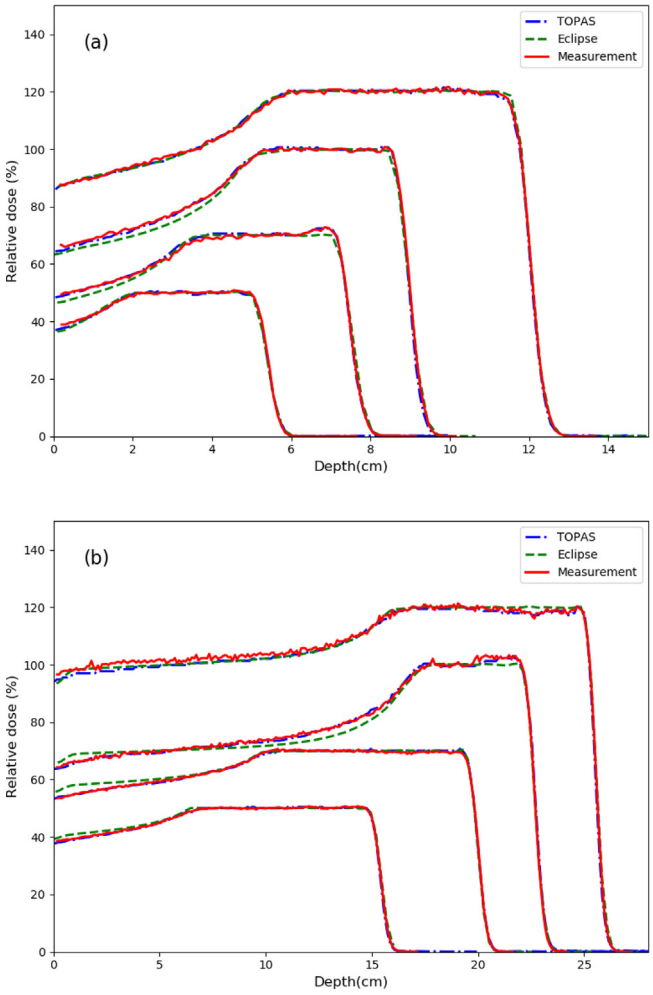

Fig. 5. Comparison of SOBP curves between the measurements (red), TPS (green), and TOPAS calculations (blue). The prescription ranges and modulation width are listed in Table 2.

typically used for our DS mode at the treatment head entrance. We used the similar approach described in literature [31]. It is reported that the spot size and angular spread have less impact on the dose distribution than the mean energy and energy spread for DS model [3]. For our DS nozzle, the second scatter is placed far enough downstream, the width of beam onto it will be dominated by first scatterer and variations in beam spot size at the nozzle entrance will not play a role [3]. Both the mean energy and energy spread of each primary incident beam were tuned by comparing with measured relative percent depth dose (PDD) of the pristine peak at the central axis. The mean energy is directly relevant to the proton range [32]. Here we adopted the clinical range R_{90}, which is defined at the distal 90% of the proton PDD profile. Energy spread is sensitive to distal dose fall-off (DDF), i.e. the distance from distal 80–20% dose level [4,29,32]. MC calculations of pristine Bragg peaks were performed iteratively by changing the mean energy and energy spread to achieve acceptable agreement (difference less than 0.05 cm) of calculated R_{90} and DDF values with measured data. A total of 33 PDDs were calculated and compared with the measurements. The PDDs were measured by using a PPC-05 parallel plate ionization chamber (IBA Dosimetry, Nuernberg-Schwarzenbruck, Germany) in the IBA Blue Phantom (IBA Dosimetry, Nuernberg-Schwarzenbruck, Germany). The collecting diameter of PPC-05 is 0.99 cm [33]. Doses along beam central axis in a water phantom were calculated in MC simulations with the resolution of 1.0 cm in diameter and 0.1 cm in depth bins. Since it's for the relative dose comparison, all calculated pristine peak curves were normalized to the corresponding peak dose.

Table 2
Comparisons of ranges, modulation widths and DDF between measurements, TPS and TOPAS calculations.

Option	Prescribed R_{90}, Width (cm)	Measured R_{90}, Width, DDF (cm)	TPS R_{90}, Width, DDF (cm)	TOPAS R_{90}, Width, DDF (cm)
B1	5.00, 3.80	5.15, 3.78,0.35	5.11, 3.83,0.42	5.15, 3.76, 0.38
B2	7.13, 4.30	7.25, 4.26, 0.41	7.23, 4.30, 0.43	7.25, 4.36, 0.41
B3	8.64, 4.30	8.69, 4.23, 0.43	8.65, 4.12, 0.48	8.67, 4.31, 0.41
B4	11.64, 7.20	11.68, 6.94, 0.48	11.70, 7.05, 0.46	11.64, 6.96, 0.48
B5	15.10, 10.40	15.05, 9.98,0.51	15.06, 10.29,0.51	15.04, 10.11, 0.50
B6	19.50, 13.00	19.59, 11.71,0.56	19.60, 11.94, 0.53	19.60, 11.97, 0.56
B7	22.10, 6.00	22.31, 6.18,0.55	22.29, 6.02,0.58	22.29, 6.34, 0.56
B8	25.00, 11.45	25.18, 11.84,0.54	25.17, 11.31, 0.55	25.17, 11.48, 0.52

2.4. Spread-out Bragg peaks and lateral profiles

As described in Section 2.2, SOBP profiles are achieved by rotating the RMW synchronized with the beam current modulation. For each SOBP calculated, the CONVALGO was used to obtain the RMW and track number, as well the corresponding modulated beam currents. For machine set-up with different range and modulation width, various RMW tracks will be implemented with modulated beam current. The RMW track was constructed as a series of steps of increasing thickness and but decreasing angular width, such as shown in Fig. 2. For each track, a brass "stop block" (black region in Fig. 2) with enough thickness is used to stop all protons. The track rotation usually starts from the "stop block", and this "start angle" is various for different RMW tracks. SOBP range and modulation width strongly depend on the "start angle" of the track, but CONVALGO can't provide the value of "start angle". It's crucial to first calibrate and verify the start angle for each track. In this study, the start angle was calibrated according to the SOBP tendency analysis [11,21]. CONVALGO-calculated nozzle setups and beam current modulations were implemented in MC simulation, with corrections made in tuned mean energy and energy spread discussed in Section 2.3. TOPAS calculated SOBPs were then compared with TPS (Eclipse version 11, Varian Medical Systems, Palo Alto, CA) calculated SOBPs and measured data. A total of 8 SOBPs, one for each of the 8 options, were calculated to commission the model in TOPAS. An aperture with opening size of 10 × 10 cm was used for all 8 cases. Like the pristine peaks, the SOBPs were measured using the PPC-05 parallel plate ionization chamber in water. The scoring resolution for SOBP calculation is the same as that for pristine peaks calculation in Section 2.3. Unlike the pristine peaks, SOBP profiles were normalized to the middle region (±0.5 cm of the middle point) of the plateau. Characteristics like clinical range R_{90}, modulation width (defined as the distance between the proximal and distal 90% dose levels) and DDF were analyzed.

In a DS nozzle, an aperture made of brass is usually used to define the treatment field shape. The position of the aperture in the beam line can also affect the field size at isocenter. To verify the aperture modeling and position, reference fields with different rectangular aperture sizes (3 × 3 cm, 6 × 6 cm and 10 × 10 cm) were simulated. These reference fields were set to have a requested range of 15.1 cm and modulation width of 10.4 cm, with source to skin distance (SSD) 220 cm and air gap (AG) of 10 cm respectively. Lateral profiles at different depths (0.5 cm, 9.9 cm and 14.1 cm) in a water phantom were measured and identically calculated in TOPAS and TPS. All measurements were performed using an electron diode (IBA Dosimetry, Nuernberg-Schwarzenbruck, Germany), with no range compensator used. This diode has an active area with diameter of 0.2 cm [33]. In MC calculations, 0.1 cm width of scoring bins was used in the field and lateral penumbra region. All of the results were normalized to the center of profile for comparison. Lateral penumbra values for all the profiles were then compared.

2.5. Range compensator verification

Treatment-field-specific range compensators (usually made of Lucite) in DS mode are used to adjust the Bragg peaks in depths and conform dose to distal edge of target [5]. To validate the modeling of RC in TOPAS and also to evaluate the corresponding dose accuracy by TPS, a test plan for a stair-shaped homogeneous water target was created in a water phantom in TPS (see Fig. 3). The left part of Fig. 3 shows the cross-section view of the range compensator thickness contour displayed in Eclipse. Different color in this figure represent the various thickness of the pixels, for example the pink region means the pixel thickness is ranging from 5 to 5.3 cm. The RC thickness data can be exported through DICOM RT Ion Plan. In this plan, the TPS calculated RC therefore features two sharp gradients at ± 3 cm from and parallel to the beam central axis, it was designed with a 0.1 cm base and 1 cm border smoothing, no smearing. The field was designed to have a prescribed range of 15.12 cm and modulation width of 9.13 cm. In our MC simulation, this RC was represented by a Lucite cylinder with a number of holes drilled out. These holes were represented as small cylinders of air inside the larger Lucite cylinder, and a hexagonal prism approximation to the cylinder was adopted to describe milling bit overlaps and improve computation efficiency [6]. The radius and positions of the holes were extracted from the RT plan exported from TPS. An in-house script was developed to automatically create the TOPAS input file for the RC model. Since TPS exports AP and RC data at the isocenter plane, a correction (using the virtual source to isocenter distance (SID), isocenter to aperture tray distance and isocenter to compensator tray distance) is required to obtain their physical dimensions [12,18]. Measurements for this case were performed in the IBA Blue phantom. The crossline profiles were measured using the electron diode at 1 cm intervals in different depths. Dose profiles at the identical depths were calculated in MC simulation and TPS, with the scoring resolution of 0.25 × 0.25 × 0.25 cm. For each profile curve, the dose was normalized to the isocenter dose. Percent depth doses (PDD) at 0, and 4.0 cm offset from the beam axis in this crossline plane were also measured with PPC-05. As described, PPC05 has a collecting diameter of 0.99 cm, integration of the voxels' dose s by TPS and MC calculation was performed for comparison. For the depth dose, normalization was performed with respect to the middle region (± 0.5 cm of the middle point) of the SOBP.

3. Results and discussion

3.1. Pristine Bragg peaks verification

Verifications of the pristine Bragg peaks were the first step to validate the beam source and geometrical model details used in TOPAS along with the physics models. A total of 33 pristine Bragg peaks which covers all therapeutic beam energies were calculated and normalized to the maximum dose respectively. Fig. 4(a) shows 8 representative curves (with nominal ranges of 4.6, 7.5, 10.5, 13.5, 16.5, 19.83, 23.0, 26.0 cm respectively) of TOPAS calculated pristine Bragg peaks compared with measured data. Primary proton histories of 2×10^8 were simulated to

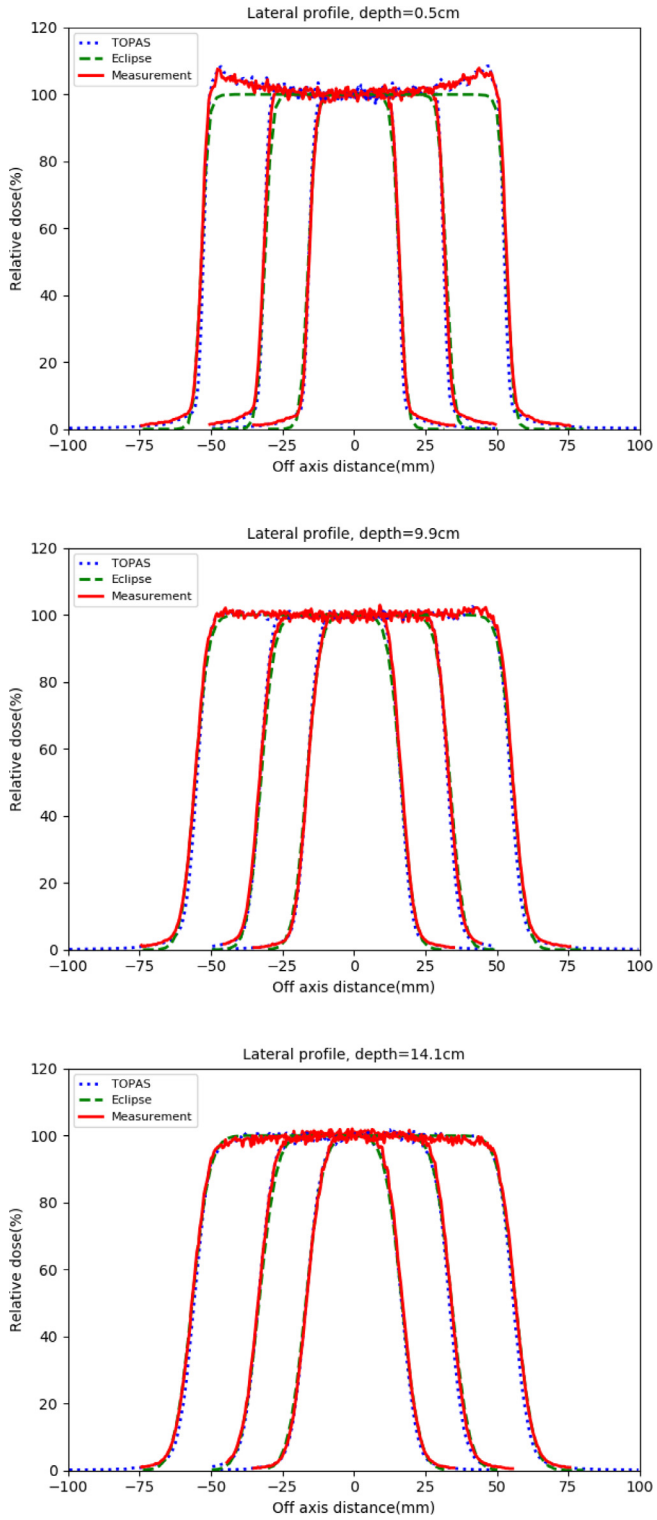

Fig. 6. Lateral profiles at different depths for various aperture opening sizes (10 × 10 cm, 6 × 6 cm and 3 × 3 cm). (a) for depth at 0.5 cm, (b) for depth at 9.9 cm and (c) for depth at 14.1 cm.

achieve statistic errors less than 0.5% for most regions of the pristine Bragg peak curve. Only in distal low dose regions (< 20% of the peak dose) statistical error can be as large as 2%. This is mainly due to that most of the primary particles have been stopped and not sufficient histories reached and were scored at the distal low dose regions. TOPAS calculations matched very well with the measurements, with maximum dose difference less than 3% in all depth bins and most of differences less than 1%. Noted that the TOPAS input beam mean energy for the simulation has been tuned to achieve agreement of calculated and measured beam range R_{90} values. Fig. 4(b) shows the ratios of TOPAS calculated R_{90} over the measured one. The maximum distance difference of R_{90} between MC calculations and measurements for all 33 curves was less than 0.03 cm, and the relative difference were less than 1%. Apart from the mean energy correction, the energy spread was adjusted to match the MC calculated DDF values to the measured ones. Linear interpolation was used to calculate the distance from distal 80–20% dose level, i.e. the DDF. Fig. 4(c) shows the DDF of the 33 pristine Bragg peaks vary with the ranges. The DDF was about several millimeters and the maximum difference between TOPAS calculation and measurement was less than 0.05 cm. We herein assume that the energy spread is the only parameter that determines the pristine Bragg peak DDF. The tuned beam mean energy and energy spread were then subsequently used for the remaining simulations.

3.2. SOBPs and lateral profiles verification

The calculation of SOBPs represents a consistency test of the RMW model, beam current modulation, TOPAS time-dependent behavior, as well as the tuned beam energy and energy spread. A total of 8 SOBPs which covers all 8 options of the DS nozzle were simulated and then compared with TPS calculated and measured data, as shown in Fig. 5. The total number of primary histories simulated was in the magnitude of 10^9 to contain calculation statistic errors under 1%, the exact number of histories being determined by the beam current modulation and is different for various options. All the SOBPs in Fig. 5 were normalized to the average of middle region (±0.5 cm of the middle point) of the dose plateau. The 8 curves in Fig. 5(a) and (b) were scaled differently to improve readability. As shown in Fig. 5, the MC simulations of SOBP were able to achieve good agreement with the measurements, even for the proximal region. Most of the dose difference was less than 2%, although the maximum difference can be 5% at the DDF region due to its high dose gradient. This is mainly due to the linear interpolation we applied to calculate the difference. The dose decrease sharply at the distal end, only few points can be used for comparison, and interpolation between these points sometimes can lead to large discrepancy. In contrast, TPS calculations in general agreed well with measurement, although with sometimes significant discrepancies at the proximal region. These discrepancies may be due both to a weakness of the analytic dose calculation algorithm and beam modeling compromises.

The SOBP comparisons demonstrated good agreement between measurements vs. TPS and TOPAS calculations. Table 2 shows the comparison of SOBP ranges R_{90}, modulation widths and DDF between measurements, TPS, and TOPAS calculations. A maximum difference of 0.04 cm for the range R_{90} and 0.5 cm for modulation width were observed when compared with measurements. The calculated DDF also matched well with the measurements, with the difference less than 0.03 cm.

For the lateral profiles, we compared doses at different depths for different aperture opening sizes (see Section 2.4). Fig. 6(a)–(c) present lateral profiles at depths of 0.5 cm, 9.9 cm and 14.1 cm for the 10 × 10 cm, 6 × 6 cm and 3 × 3 cm aperture opening size, respectively. We choose those depths to represent the entrance, middle and distal end of the SOBP. TOPAS simulated lateral profiles resulted in better than 3% dose agreement on average with the measured data for all depths, with the overall statistical error less than 3%. Even at the entrance depth of 0.5 cm, where the measured profiles show “horns” at both side near the field edges, TOPAS calculation agreed well with measurements. TPS analytic dose calculation algorithm, predictably, failed to accurately predict the “horns” produced by the “slit scattering” of protons on aperture edges [34,35]. Apart from that, at the very low dose edge (< 5%) of the profile outside the field, the measurements showed a nearly linear decrease in dose level from about 5–0% over a distance of about 1 cm, whereas the TPS calculation simply decrease

Table 3
The lateral penumbra for measurements, TPS and TOPAS.

AP opening size (cm)	Depth at 0.5 cm			Depth at 9.9 cm			Depth at 14.1 cm		
	Measured	TPS	TOPAS	Measured	TPS	TOPAS	Measured	TPS	TOPAS
3 × 3	0.323	0.365	0.294	0.572	0.648	0.541	0.776	0.829	0.731
6 × 6	0.328	0.368	0.296	0.585	0.643	0.556	0.785	0.837	0.776
10 × 10	0.324	0.371	0.284	0.618	0.652	0.587	0.792	0.842	0.750

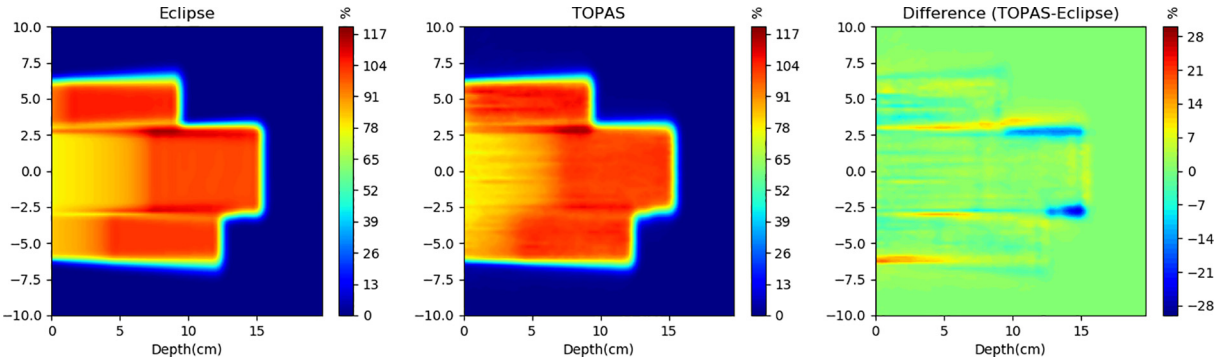

Fig. 7. Relative dose distributions at the transversal plane of TPS and TOPAS calculations. The right figure is the difference by TOPAS minus Eclipse calculation.

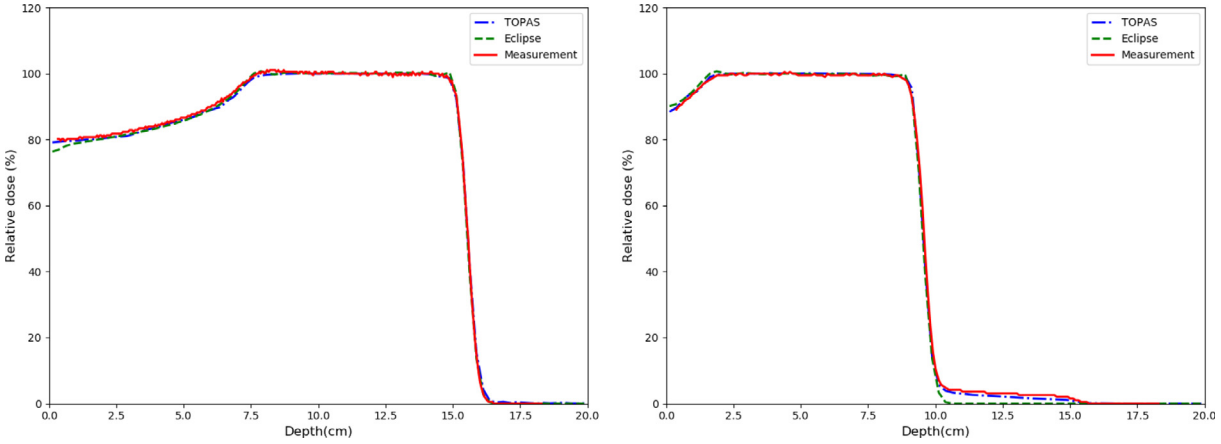

Fig. 8. Comparison of percent depth doses at 0 (left) and 4.0 cm (right) offset from the beam axis.

sharply at that region. This under-estimate of dose outside the field is most apparent in the case with small aperture opening size and at shallower depths. Protons that interact with the vertical slit surfaces of an aperture with a finite thickness will lose energy and scatter, but may not be totally stopped. These scattered low energy protons tend to converge towards beam axis with a small angle (typically 6°) [35]. The increase of fluence inside and near the field edge will thus result in the "horn effect". Slit scattering can be only described using electromagnetic (EM) stopping and scattering theory [35], which has been incorporated in TOPAS default physics list [27]. Pencil beam algorithms are unable to predict this effect correctly. These low energy protons are also responsible for the slightly increased dose tails immediately outside the field. The lateral fluence spread in TPS is calculated according to the aperture contours projected at isocenter, and assumes an infinitely thin aperture [12]. This effect is therefore not modeled in analytical methods, but can be correctly predicted in MC simulations. The differences between MC simulations, TPS calculations and measurements were reduced with the increase of depth.

Our TOPAS DS nozzle model also achieved very good agreement (better than 0.1 cm) of the lateral penumbras between measurements, TPS, and MC simulations. Table 3 presents the lateral penumbras for each aperture at various depths in water, where the three penumbra values of each cell correspond to measurement, TPS and TOPAS calculation respectively. Lateral penumbra values are only several millimeters for all scenarios. A sharp lateral penumbra is essential for sparing the critical organs adjacent to the target volume. This is also one of the most attractive features of the DS proton therapy. No significant differences of lateral penumbra values at the same depth were observed for various AP opening sizes. Lateral penumbra increase dramatically with the depth. For protons, the main interacting mechanism is multiple Coulomb scattering (MCS) [10,12,13]. A proton changes its direction very little after each interaction, but this change accumulates rapidly and increases the beam penumbra as the beam traverses deeper. As shown in Table 3, the TOPAS calculated penumbra values are slightly lower than measurement, while TPS overestimated the values. For TOPAS result, a possible reason for this difference of lateral penumbra between calculated and measured data is the small air gap (usually less than 1 cm) between snout and aperture, which is not considered in our TOPAS model. The lateral penumbra values are very sensitive to the air gap, though there is no significant difference observed in the profiles. While for TPS calculations, the previously mentioned fail to model the slit scattering in TPS can be responsible for this issue. Without considering the convergence of these scattered protons, TPS will underestimate the dose near the "horn" region, and this could

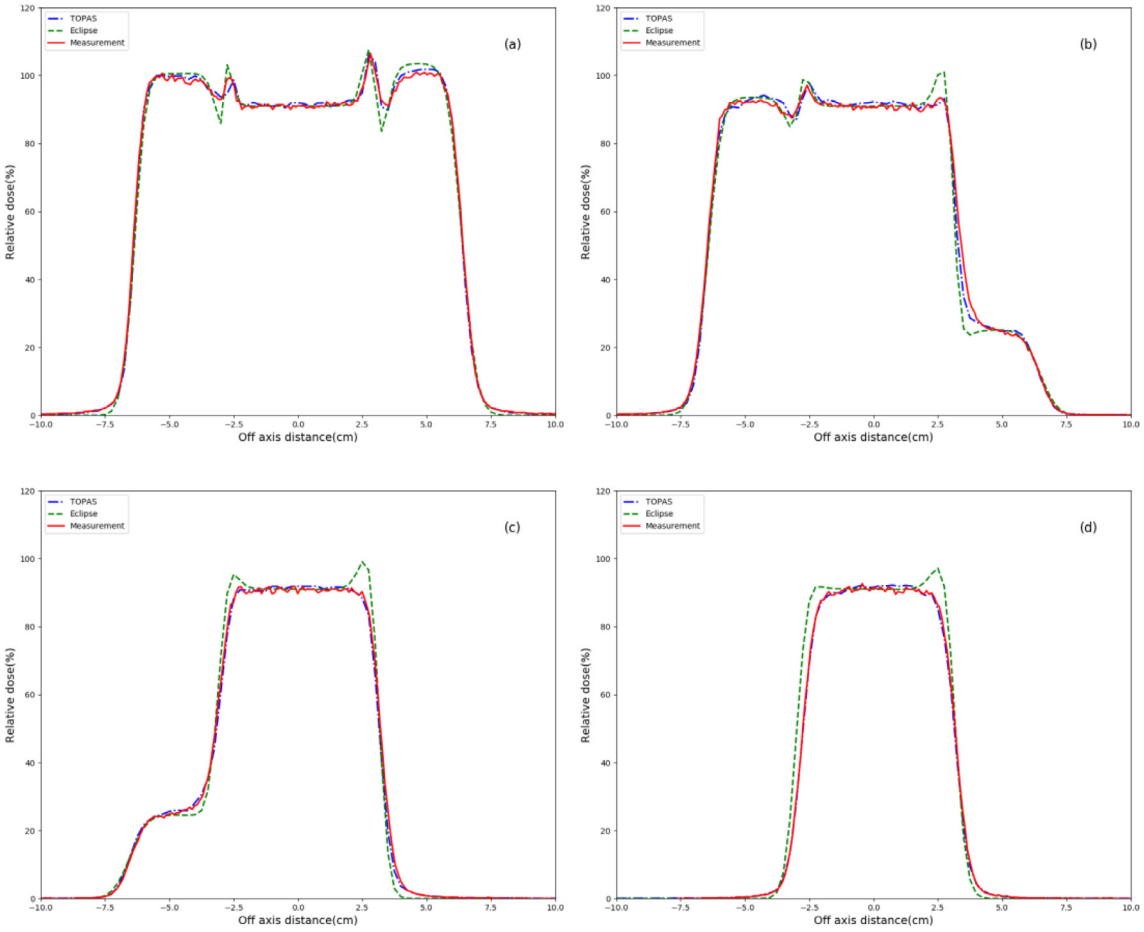

Fig. 9. Comparison of profiles perpendicular to the beam incident direction at different depths. Figure (a)–(d) are for depth at 6.7, 9.7, 12.7 and 14.7 cm respectively.

lead to the increase of 80–20% penumbra values.

3.3. Range compensator verification

Fig. 7 compares TOPAS vs. TPS calculated dose distributions in the transversal plane for the stair target case. The left figure is the TPS calculation, middle is the TOPAS calculation and the right figure is the difference by TOPAS subtracting TPS calculation. All of them were normalized to the isocenter. The overall statistical error for this planar dose calculation by TOPAS was less than 2%. As shown in Fig. 7, in most regions TPS predicted the dose distribution consistently with the TOPAS calculation, the ranges of the three different depths matched very well with the MC calculation, which means the range pullback effect by RC is properly modeled in TPS. TPS calculated dose is approximately 10% lower than MC simulation outside the target, while it can overestimate the dose by up to 25% immediately inside the target volume.

Two representative depth dose curves at 0 and 4.0 cm offset from the beam axis was calculated and then compared with the PPC-05 measurements, as shown in Fig. 8. Both of the two SOBP curves in Fig. 8 by TPS and TOPAS calculation are generally in good agreement with the measurements. The SOBP ranges and modulation widths predicted by TPS and TOPAS also agreed within 0.03 cm of the measured data, which means the material and thickness of RC were correctly addressed in TOPAS and TPS. For the PDD at 4.0 cm in right part of Fig. 8, the additional dose deposited behind the SOBP in measured data shows a slowly decrease till the prescribed range 15.12 cm. TOPAS in general predicted this effect very well, though with somehow underestimation. While TPS analytical algorithm models with a sharp dose decrease to zero. This effect can be also observed from the difference map in Fig. 7. The weakness of nuclear halo modelling in TPS can be responsible for this effect. According to Eclipse algorithm reference guide, RC is modeled as an element of the beam line, since the air gap correction should be considered [12].The lateral fluence including RC effects in Eclipse is calculated as following [12]:

$$\Phi^{final}(x, y, z) = \iint \Phi(x, y, z) \cdot \frac{1}{2\pi {\sigma_c}^2} \cdot \exp\left(\frac{(x-x)^2 + (y-y)^2}{2{\sigma_c}^2}\right) dx\, dy \tag{1}$$

where $\Phi(x, y, z)$ is the in air fluence without RC, final means the fluence after RC. σ_c is the rms width of the spatial distribution of protons scattered in RC, it can be calculated by:

$${\sigma_c}^2 = \Theta(x, y) \cdot Z_{RC} \tag{2}$$

where Θ is the MCS characteristic angle in the Highland formalism, Z_{RC} is the distance between the center of RC voxel to the point of calculation. As seen from this formula, lateral scattering in the compensator is basically included in the TPS analytical algorithm, but only take the MCS into account, which means that protons undergo large angle scattering have been ignored [12]. While large angle scattering is correctly modeled in TOPAS physics list, and this effect can be clearly distinguished in the additional dose tail presented in Fig. 8 right part.

TOPAS and TPS calculated lateral profiles were also compared to measured data in order to further validate their accuracies. Fig. 9 shows lateral profiles at depths of 6.7, 9.7, 12.7 and 14.7 cm, the blue line is the TOPAS calculation, the green line is the Eclipse calculation and the red line is the measurement. All of the profiles have been normalized to the isocenter. For the low dose region outside the target, TPS calculation is lower than the measurement, with the maximum dose difference up to 10%. While the counterpart in MC simulation agree well with

measurement, with the maximum difference less than 2%. As described in Section 3.3, this discrepancy is mainly due to the protons transverse the downstream of AP, which is not modeled in analytical algorithms. Inside target volume, TPS predicted dose distributions correctly to a large extent, even for the "double spikes" at the boundaries between target steps (see profiles at 6.7 cm). This "double spikes" effect was mainly due to protons scattered out of the thicker step region and into the thinner step. It results in increase of fluence at the thinner part of the boundary and correspondingly decreased fluence at the thicker part. At deeper depth, for example at 14.7 cm, TOPAS calculated dose profile agreed well with measurements with relative difference less than 5%, whereas TPS overestimates dose immediately inside target by up to 25%, where the large heterogeneity of RC was encountered. A possible explanation for the significant difference is the analytical algorithm implemented in TPS. As described in formula 1, the effect of the scattering in the RC is modeled as a perturbation of the proton in-air fluence, and only the MCS is considered [12]. The effect of fluence perturbation caused by RC thickness variations is decoupled from depth dose calculation in analytical dose algorithm [12]. Analytical algorithm does not model the fact that protons scattered in a thick step lose part of their energy and its effects on depth dose distribution. It is therefore expected that this effect will become obvious when steep gradient is present in the RC or high tissue inhomogeneity is encountered in the beam path.

4. Conclusion

In this study, we have presented a DS nozzle model specifically developed and commissioned in TOPAS to accurately calculate dose distributions in a water phantom. The geometrical model was built based on the blueprint provided by the manufacturer of our proton therapy system. The initial beam source model was fine-tuned to match Bragg Peak PDDs with measurements. The commissioned model was then implemented to calculate SOBPs for all 8 beam energy options, as well as lateral profiles for various field sizes. A stair-shaped target test plan with highly inhomogeneous RC was then simulated to evaluate the performance of dose accuracy for TPS analytical algorithm and TOPAS MC code. It has shown that the MC based DS nozzle model we developed can produce more accurate dose distributions in a water phantom than the TPS analytical algorithm when compared to the measurements, especially for the case with highly heterogeneous RC. It is found that the TPS can overestimate the relative dose by up to 25% while MC calculations predicted the dose to within 5% of measurements. Therefore, this MC model we developed has the potential to be a useful tool in clinical for dosimetric verification in DS modality. Further study would follow up with patient treatment plan verification based on this commissioned model.

Acknowledgements

This work was jointly supported by the following grants: National Natural Science Foundation of China (No. 11575180), National key research and development plan (No. 2017YFC0107500), Anhui key research and development plan (No. 1804a09020039).

The first author, Hongdong Liu, a PhD candidate at USTC, was supported by a China Scholarship Council (CSC) grant as a one-year exchange student to perform his dissertation research project at University of Florida Health Proton Therapy Institute. The authors would also like to thank Ion Beam Applications for providing us with the Universal Nozzle data and fruitful discussions.

References

[1] Particle Therapy Cooperative Group (PTCOG) 2018 Particle therapy facilities in a planning stage or under construction (last update: January 2019). http://ptcog.web.psi.ch/newptcentres.

[2] Particle Therapy Cooperative Group (PTCOG) Particle Therapy Patient Statistics (per end of 2017). http://ptcog.web.psi.ch/patient statistics.

[3] Slopsema R. "Beam, delivery using passive scattering". CRC Press 2016. https://doi.org/10.1201/b11448.

[4] Lu HM, Flanz J. "Characteristics of Clinical Proton Beams". CRC Press 2016. https://doi.org/10.1201/b11448.

[5] Mohan R, Grosshans D. Proton therapy–present and future. Adv Drug Deliv Rev 2017;109:26–44. https://doi.org/10.1016/j.addr.2016.11.006.

[6] Perl J, Shin J, Schümann J, et al. TOPAS: An innovative proton Monte Carlo platform for research and clinical applications. Med Phys 2012;39(11):6818–37. https://doi.org/10.1118/1.4758060.

[7] Clair WHS, Adams JA, Bues M, et al. Advantage of protons compared to conventional X-ray or IMRT in the treatment of a pediatric patient with medulloblastoma. Int J Radiat Oncol Biol Phys. 2004;58(3):727–34. https://doi.org/10.1016/S0360-3016(03)01574-8.

[8] Chang JY, Jabbour SK, De Ruysscher D, et al. Consensus statement on proton therapy in early-stage and locally advanced non–small cell lung cancer. Int J Radiat Oncol* Biol* Phys 2016;95(1):505–16. https://doi.org/10.1016/j.ijrobp.2016.01.036.

[9] Hong L, Goitein M, Bucciolini M, et al. A pencil beam algorithm for proton dose calculations. Phys Med Biol 1996;41(8):1305. https://doi.org/10.1088/0031-9155/41/8/005.

[10] Soukup M, Fippel M, Alber M. A pencil beam algorithm for intensity modulated proton therapy derived from Monte Carlo simulations. Phys Med Biol 2005;50(21):5089. https://doi.org/10.1088/0031-9155/50/21/010.

[11] Bäumer C, Geismar D, Koska B, et al. Comprehensive clinical commissioning and validation of the RayStation treatment planning system for proton therapy with active scanning and passive treatment techniques. Phys Med 2017;43:15–24. https://doi.org/10.1016/j.ejmp.2017.09.136.

[12] Varian, Proton Algorithm Reference Guide (Varian Medical Systems, Palo Alto, CA, 2011).

[13] RaySearch, RayStation 6 Reference Manual (RaySearch Laboratories, Stockholm, Sweden, 2016).

[14] Paganetti H, Jiang H, Lee SY, et al. Accurate Monte Carlo simulations for nozzle design, commissioning and quality assurance for a proton radiation therapy facility. Med Phys 2004;31(7):2107–18. https://doi.org/10.1118/1.1762792.

[15] Chen H, Matysiak W, Flampouri S, et al. Dosimetric evaluation of hybrid brass/stainless-steel apertures for proton therapy. Phys Med Biol 2014;59(17):5043. https://doi.org/10.1088/0031-9155/59/17/5043.

[16] Taylor PA, Kry SF, Followill DS. Pencil beam algorithms are unsuitable for proton dose calculations in lung. Int J Radiat Oncol Biol Phys 2017;99(3):750–6. https://doi.org/10.1016/j.ijrobp.2017.06.003.

[17] Schuemann J, Giantsoudi D, Grassberger C, et al. Assessing the clinical impact of approximations in analytical dose calculations for proton therapy. Int J Radiat Oncol Biol Phys 2015;92(5):1157–64. https://doi.org/10.1016/j.ijrobp.2015.04.006.

[18] Shin WG, Testa M, Kim HS, et al. Independent dose verification system with Monte Carlo simulations using TOPAS for passive scattering proton therapy at the National Cancer Center in Korea. Phys Med Biol 2017;62(19):7598. https://doi.org/10.1088/1361-6560/aa8663.

[19] Beltran C, Jia Y, Slopsema R, et al. A simplified methodology to produce Monte Carlo dose distributions in proton therapy. J Appl Clin Med Phys 2014;15(4):2–10. https://doi.org/10.1120/jacmp.v15i4.4413.

[20] Schuemann J, Dowdell S, Grassberger C, et al. Site-specific range uncertainties caused by dose calculation algorithms for proton therapy. Phys Med Biol 2014;59(15):4007. https://doi.org/10.1088/0031-9155/59/15/4007.

[21] Testa M, Schumann J, Lu HM, et al. Experimental validation of the Topas Monte Carlo system for passive scattering proton therapy. Med Phys 2013;40(12):121719https://doi.org/10.1118/1.4828781.

[22] Chung K, Kim J, Kim DH, et al. The proton therapy nozzles at samsung medical center: a Monte Carlo simulation study using TOPAS. J Korean Phys Soc 2015;67(1):170–4. https://doi.org/10.3938/jkps.67.170.

[23] Agostinelli S, Allison J, Amako K, et al. GEANT4—a simulation toolkit. Nucl Instrum Methods Phys Res Sect A: Accel, Spec, Detectors Associated Equipment 2003;506(3):250–303. https://doi.org/10.1016/S0168-9002(03)01368-8.

[24] Schümann J, Paganetti H, Shin J, et al. Efficient voxel navigation for proton therapy dose calculation in TOPAS and Geant4. Phys Med Biol 2012;57(11):3281. https://doi.org/10.1088/0031-9155/57/11/3281.

[25] Shin J, Perl J, Schümann J, et al. A modular method to handle multiple time-dependent quantities in Monte Carlo simulations. Phys Med Biol 2012;57(11):3295. https://doi.org/10.1088/0031-9155/57/11/3295.

[26] Ramos Mendez J, Perl J, Faddegon B, et al. Geometrical splitting technique to improve the computational efficiency in Monte Carlo calculations for proton therapy. Med Phys 2013;40(4). https://doi.org/10.1118/1.4795343.

[27] Jarlskog CZ, Paganetti H. Physics settings for using the Geant4 toolkit in proton therapy. IEEE Trans Nucl Sci 2008;55(3):1018–25. https://doi.org/10.1109/TNS.2008.922816.

[28] Lu HM, Kooy H. Optimization of current modulation function for proton spread-out Bragg peak fields. Med Phys 2006;33(5):1281–7. https://doi.org/10.1118/1.2188072.

[29] Shin J, Kim D, Lim YK, et al. Monte Carlo modeling and simulation of a passive treatment proton beam delivery system using a modulation wheel. J Korean Phys Soc 2010;56(1):153–63. https://doi.org/10.3938/jkps.56.153.

[30] Pérez-Andújar A, Newhauser WD, DeLuca Jr. PM. Neutron production from beam-modifying devices in a modern double scattering proton therapy beam delivery system. Phys Med Biol 2009;54(4):993. https://doi.org/10.1088/0031-9155/54/4/

012.
[31] Paganetti H, Jiang H, Parodi K, et al. Clinical implementation of full Monte Carlo dose calculation in proton beam therapy. Phys Med Biol 2008;53(17):4825. https://doi.org/10.1088/0031-9155/53/17/023.
[32] Gottschalk B. Passive Beam Spreading in Proton Radiation Therapy (Draft Oct 2004). 2004. Available from: https://gray.mgh.harvard.edu/attachments/article/212/pbs.pdf.
[33] IBA Dosimetry, Ionization chambers and diode detectors - Detectors for relative and absolute dosimetry. Available from: https://www.iba-dosimetry.com/radiation-therapy/detectors.
[34] Slopsema RL, Kooy HM. Incorporation of the aperture thickness in proton pencil-beam dose calculations. Phys Med Biol 2006;51(21):5441. https://doi.org/10.1088/0031-9155/51/21/004.
[35] Gottschalk B. Slit scattering. 2008. Available from: https://gray.mgh.harvard.edu/attachments/article/213/17_SlitScattering.ppt.